Evaluation of the orientation relations from misorientation between inherited variants: Application to ausformed martensite

Michel Humbert, Lionel Germain, Nathalie Gey, Elodie Boucard

Evaluation of the orientation relations from misorientation between inherited variants: Application to ausformed martensite

M. Humbert,[a] L. Germain,[a,b,*] N. Gey[a,b] and E. Boucard[a,b]

[a] *Laboratoire d'Etude des Microstructures et de Mécanique des Matériaux (LEM3), UMR 7239, CNRS/Université de Lorraine, F-57045 Metz, France*

[b] *Laboratory of Excellence on Design of Alloy Metals for low-mAss Structures ("LabEx DAMAS"), Université de Lorraine, France*

Abstract—This paper describes a way to deduce the orientation relation occurring in phase transformation by only considering three misorientations between variants inherited from the same parent grain at a triple point. The method, named XABX, can be successfully applied even in materials deformed before phase transformation. This new approach, developed for investigating orientation relations in steels, is easily transposable for studying orientation relations of other phase transformations.

Keywords: Phase transformations; Variants; Orientation relation determination; Steels

1. Introduction

Phase transformations strongly influence the microstructures of materials and consequently their mechanical properties through the orientation relations (ORs) between parent and child phases and spatial arrangement of selected variants. Therefore, the knowledge of accurate characteristics of the phase transformations is important. In this framework, the most precise determination of the ORs allows us to investigate the phase transformation conditions and types. For example, in steel transformations, the ORs between austenite and the child phase can be different from the classical Nishiyama–Wassermann (NW) or Kurdjumov–Sachs (KS) ORs [1–7]. The direct determination of the ORs requires that a sufficient amount of the parent phase is retained at room temperature [1,2]. When this is not the case, the evaluation of the OR can be performed by considering the coincidence of high indices pole figures (PFs) of experimental and calculated data [3,4,8]. Using this procedure in a first step, Miyamoto et al. [8] presented a numerical method to evaluate the OR occurring in the steel phase transformation. Following a similar approach, an analytical method to determine the OR has also been proposed [9]. Until now, all methods operating without retained parent phase implicitly assume that the orientation is constant within the parent grain. However, in deformed materials, orientation gradients exist. In the presence of such orientation variations, the later methods do not correctly operate. The method presented here applies even when the later methods do not operate correctly. It uses the local misorientations between variants to deduce the OR between the vanished parent and the child phase. We have named this method XABX after the formulae which allow the problem to be solved. Two application examples are presented: one to validate the method on a synthetic microstructure, the other on ausformed martensite.

* Corresponding author at: Laboratoire d'Etude des Microstructures et de Mécanique des Matériaux (LEM3), UMR 7239, CNRS/Université de Lorraine, F-57045 Metz, France. Tel.: +33 38731 5389; fax: +33 38731 5370; e-mail: lionel.germain@univ-lorraine.fr

2. Working hypotheses and equations

In this section, we derive the equations that allow the determination of the OR under two hypotheses. These hypotheses are further discussed in Section 4.

Let us consider the parent grain whose boundaries are the bold line shown in Fig. 1. The orientation of a point located at r_i is characterized by a rotation matrix $[g_\gamma(r_i)]$. After complete transformation, this parent grain transforms into several spatial domains (variants) whose boundaries are the thin lines. The variant orientations are defined by rotation matrices $[g_\alpha(r_i)]$.

In general, the relation between the parent and the child orientations can be expressed by a product of rotation matrices:

$$[g_\alpha(r_i)] = [g_\gamma(r_i)][P(r_i)][\Delta g(r_i)][C(r_i)] \quad (1)$$

in which $[P(r_i)]$ is one element of the n_P rotational symmetry elements of the parent phase, $[C(r_i)]$ one element of the n_C rotational symmetry elements of the child phase and the rotation $[\Delta g(r_i)]$ corresponds to the OR between the parent and the child phase at location r_i.

Let us now consider three points $[r_1, r_2, r_3]$ located at a triple point which belong to the same parent grain (Fig. 1). The links between parent and child orientations read:

$$\begin{aligned}[g_\alpha(r_1)] &= [g_\gamma(r_1)][P(r_1)][\Delta g(r_1)][C(r_1)]\\ [g_\alpha(r_2)] &= [g_\gamma(r_2)][P(r_2)][\Delta g(r_2)][C(r_2)]\\ [g_\alpha(r_3)] &= [g_\gamma(r_3)][P(r_3)][\Delta g(r_3)][C(r_3)]\end{aligned} \tag{2}$$

The first hypothesis we made is that the parent orientations do not vary (or only vary very slightly) across the variant boundaries:

$$[g_\gamma(r_1)] = [g_\gamma(r_2)] = [g_\gamma(r_3)] = [g_\gamma] \tag{3}$$

The constancy of $[g_\gamma]$ in the vicinity of a triple point allows Eqs. (2) to be combined so that $[g_\gamma]$ disappears.

After some easy manipulations, the following expressions can be found:

$$\begin{aligned}[g_\alpha(r_2)]^{-1}[g_\alpha(r_1)] &= ([P_2][\Delta g(r_2)][C_2])^{-1}([P_1][\Delta g(r_1)][C_1])\\ [g_\alpha(r_3)]^{-1}[g_\alpha(r_1)] &= ([P_3][\Delta g(r_3)][C_3])^{-1}([P_1][\Delta g(r_1)][C_1])\\ [g_\alpha(r_2)]^{-1}[g_\alpha(r_3)] &= ([P_3][\Delta g(r_3)][C_3])^{-1}([P_2][\Delta g(r_2)][C_2])\end{aligned} \tag{4}$$

At this stage, a second hypothesis is introduced. We assume that the local ORs remain close to each other and thus close to a mean OR:

$$[\Delta g(r_i)] \cong \overline{[\Delta g]}$$

This leads to a replacement of Eqs. (4) by:

$$\begin{aligned}[g_\alpha(r_2)]^{-1}[g_\alpha(r_1)] &\cong ([P_2]\overline{[\Delta g]}[C_2])^{-1}([P_1]\overline{[\Delta g]}[C_1])\\ [g_\alpha(r_3)]^{-1}[g_\alpha(r_1)] &\cong ([P_3]\overline{[\Delta g]}[C_3])^{-1}([P_1]\overline{[\Delta g]}[C_1])\\ [g_\alpha(r_3)]^{-1}[g_\alpha(r_2)] &\cong ([P_3]\overline{[\Delta g]}[C_3])^{-1}([P_2]\overline{[\Delta g]}[C_2])\end{aligned} \tag{5}$$

To simplify the notation we put $[P_1]\overline{[\Delta g]}[C_1] = \overline{[\Delta g']}$, which corresponds to an equivalent mean OR.

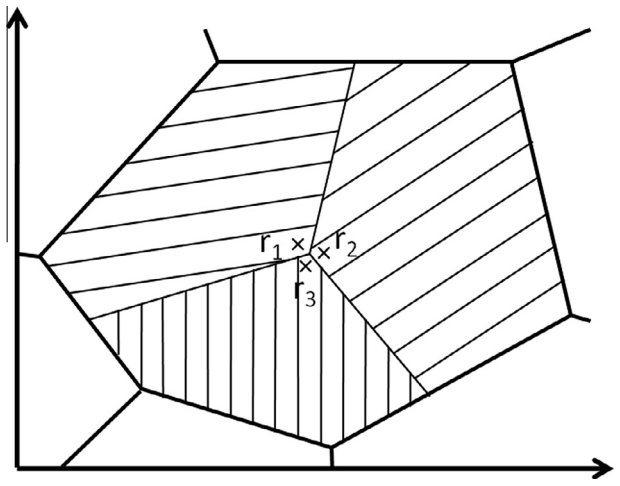

Fig. 1. The points of interest are located at a triple junction between three variants inherited from the same parent grain.

Then Eqs. (5) become:

$$\begin{aligned}[g_\alpha(r_2)]^{-1}[g_\alpha(r_1)] &\cong ([P'_2]\overline{[\Delta g']}[C'_2])^{-1}\overline{[\Delta g']}\\ [g_\alpha(r_3)]^{-1}[g_\alpha(r_1)] &\cong ([P'_3]\overline{[\Delta g']}[C'_3])^{-1}\overline{[\Delta g']}\\ [g_\alpha(r_3)]^{-1}[g_\alpha(r_2)] &\cong ([P'_3]\overline{[\Delta g']}[C'_3])^{-1}\left([P'_2]\overline{[\Delta g']}[C'_2]\right)\end{aligned} \tag{6}$$

which can be reformulated as:

$$\begin{aligned}\overline{[\Delta g']}[C'_2][g_\alpha(r_2)]^{-1}[g_\alpha(r_1)] &\cong [P'_2]^{-1}\overline{[\Delta g']}\\ \overline{[\Delta g']}[C'_3][g_\alpha(r_3)]^{-1}[g_\alpha(r_1)] &\cong [P'_3]^{-1}\overline{[\Delta g']}\\ \overline{[\Delta g']}[C'_3][g_\alpha(r_3)]^{-1}[g_\alpha(r_2)][C'_2]^{-1} &\cong [P'_3]^{-1}[P'_2]\overline{[\Delta g']}\end{aligned} \tag{7}$$

In this system, the inputs are the misorientations between three variants; the unknowns are $\overline{[\Delta g']}$ and the symmetry elements.

3. Orientation relation calculation

The general form of Eqs. (7) is $X \times A_i \cong B_i \times X$ (hence the name given to our the method) where A_i and B_i are functions of experimental data and of rotational symmetry elements and X stands for $\overline{[\Delta g']}$.

In this case, the mean local OR X, $\overline{[\Delta g']}$, must minimize the following error function:

$$E = \sum_i \|X \times A_i - B_i \times X\|^2 \tag{8}$$

with the constraint $\|X\|^2 = 1$ because X is a rotation matrix. In these expressions, $\|\|$ defines the Euclidean norm. The error function E is null if Eqs. (7) are equalities. But E may differ slightly from zero in the case of a small gradient of the parent orientation and/or in the case of variations of the local ORs.

The way to find out the value X which minimizes the error function E (Eq. (8)) is described in the Appendix. It passes through the use of quaternions whose properties are well adapted for this type of equation [10]. As shown in the Appendix A, the error function can be associated to a real positive (4×4) matrix whose components are function of the quaternions representing the rotations A_i and B_i. The four eigenvalues of this matrix (sorted from the largest: λ_1 to the smallest: λ_4) determine four values of the error function: λ_4 leads to the smallest value of Eq. (8) and its corresponding eigenvector stands for the OR X.

The symmetry elements P'_i and C'_i entering A_i and B_i are a priori not known. Therefore to find out X, we minimize the error function (Eq. (8)) for all combinations (C'_2, C'_3, P'_2, P'_3) of the n_P symmetry elements $[P_i]$ and n_C symmetry elements $[C_i]$. So the number of these calculations is $n_T = (n_C \times n_P)^2$.

Some data analysis is required to retain only the real OR among the n_T results. Let $\lambda_{4\min}$ be the minimum of the n_T λ_4s. All results having λ_4 close to $\lambda_{4\min}$ are potential solutions. If one of the potential solutions has λ_3 very close to λ_4, the system is underdetermined. In other words, it cannot be solved because at least two identical misorientations have been given as input data. If $\lambda_{4\min}$ is greater than λ_{4CRIT} then no OR relation exists within a given tolerance. The choice of λ_{4CRIT} is related to the deviation with which Eqs. (7) is respected; this is discussed in Section 4.

The potential solutions should be filtered because they contain symmetry equivalents of the OR. The remaining

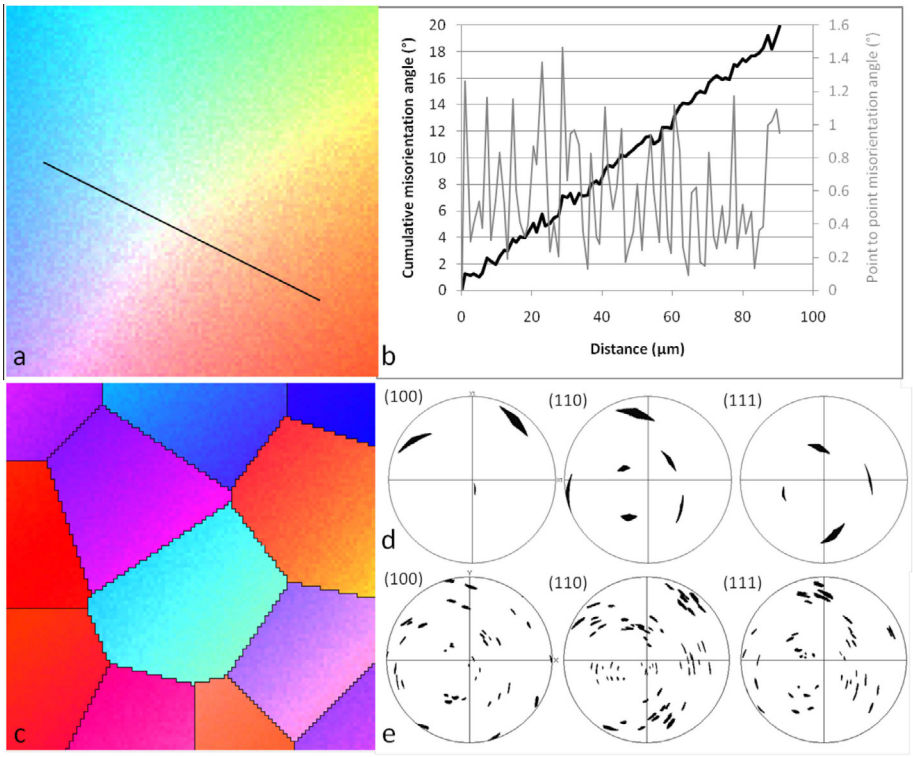

Fig. 2. (a) Synthetic γ EBSD map. (b) Misorientation profiles along the black line of (a). (c) EBSD map of the α phase after transformation with KS relationship. (d and e) The pole figures respectively of the γ phase and the α phase.

potential solutions correspond to ORs that relate the orientation of the three variants to a unique parent orientation (within a certain tolerance). If the solution is unique, it is the true solution.

The reliability of the method was first tested thanks to simulated data, using the Greninger–Troiano (GT) OR ($\Delta g = (2.679°, 47.06°, 7.573°)$). The orientations of the 24 GT variants with $[g_\gamma(r)] = I$ were calculated, I being the identity matrix. Theoretically, 2024 combinations of three different variants are possible; however, only 1920 present three distinct misorientations. The potential solutions have been obtained using the following condition:

$$\frac{\max(\lambda_4, 10^{-15}) - \max(\lambda_{4\min}, 10^{-15})}{\max(\lambda_4, 10^{-15})} < 0.9$$

The max functions are here to account for a negative value of λ_4, which may occur due to numerical precision. λ_{4CRIT} was chosen equal to 6×10^{-4}.

The XABX method was applied to each of the 1920 combinations. 1248 combinations (65%) gave the GT OR. For the other combinations, multiple solutions were found (in which the GT OR is always included).

The results can be improved considering that ORs in steel are close to KS, NW, GT or Pitch ORs. After filtering out solutions not contained in a domain bounded by KS, NW and Pitch, the GT OR was found in the 1848 case (96.25%). For all combinations, $\lambda_{4\min}$ was lower than 2×10^{-15}, so any choice of $\lambda_{4CRIT} > 2 \times 10^{-15}$ does not change the results.

This numerical testing shows that, for a large majority of the combinations, the exact solution is found. Of course, here neither orientation gradient nor noise was introduced in the data.

4. Applications

The XABX method can be easily applied to electron backscatter diffraction (EBSD) maps. We present results on two examples. First is a synthetic EBSD map designed with a gradient and some noise in the parent orientation. Our purpose is to validate the method in the case where the expected result is known. In the second example, the method was applied to two ausformed martensite microstructures: one quenched directly after deformation and the other annealed for recrystallization before quenching. The transformation conditions were identical for both microstructure (chemistry, cooling rate, grain size) and thus the OR should be very similar.

4.1. Synthetic microstructure with orientation gradient

In the first example, we produced a synthetic EBSD map of 100×100 pixels to validate our approach. The EBSD map represents a part of a parent γ grain with a gradient texture. The orientation, $g_\gamma(x,y)$, of each pixel was obtained using the following simple function of Euler angles in degrees:

$$\varphi_1(x,y) = 10 + 15x/x\max$$

$$\Phi(x,y) = 20 - 15(3x + y)/(3x\max + y\max)$$

$$\varphi_2(x,y) = 30 + 15y/y\max$$

Two cases have been considered: one without noise, one with noise. The noise was introduced by adding a random number between $-0.5°$ and $0.5°$ to each Euler angle. The initial data and the result are illustrated in Fig. 2 for the

Table 1. Effect of input data on the OR determinations from the EBSD map of Fig. 2c.

	Without noise	With noise
Use of misorientations at triple points	$\Delta g = (5.55°, 48.17°, 5.94°)$ $\lambda_4 < 6.10^{-6}$ Angle with KS = 0.173°	$\Delta g = (5.42°, 48.1°, 6.05°)$ $\lambda_4 < 2.10^{-4}$ Angle with KS = 0.265°
Use of average misorientation along boundaries	$\Delta g = (5.64°, 48.17°, 5.85°)$ $\lambda_4 < 4.10^{-6}$ Angle with KS = 0.109°	$\Delta g = (5.79\ 48.207\ 5.713°)$ $\lambda_4 < 3.10^{-5}$ Angle with KS = 0.097°

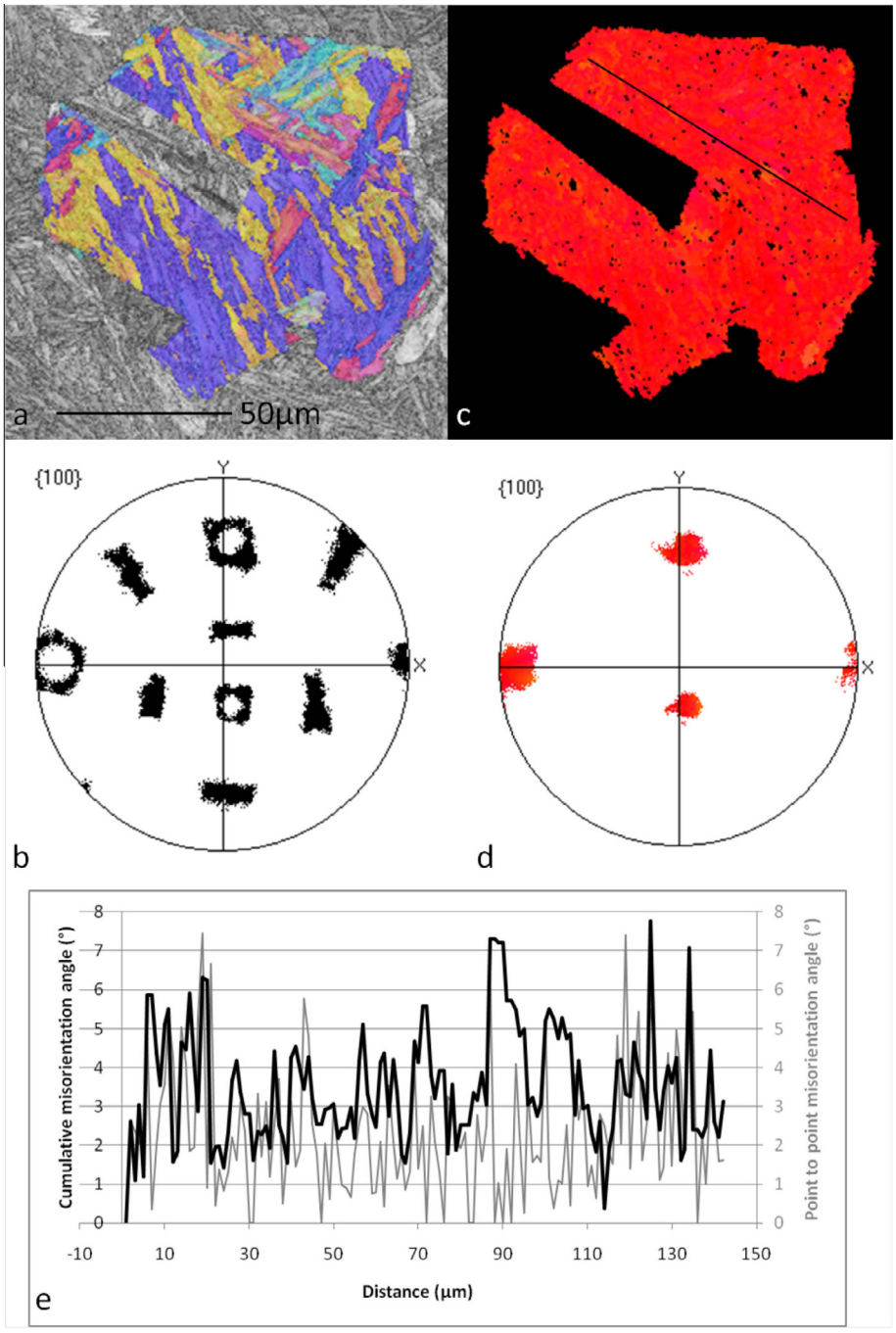

Fig. 3. (a) EBSD map of α variants in a recrystallized parent austenite grain in IPF, (b) {100} pole figure of the α variants, (c) the reconstructed γ grain, (d) {100} pole figure of the reconstructed γ grain and (e) misorientation profiles along the black line in (c).

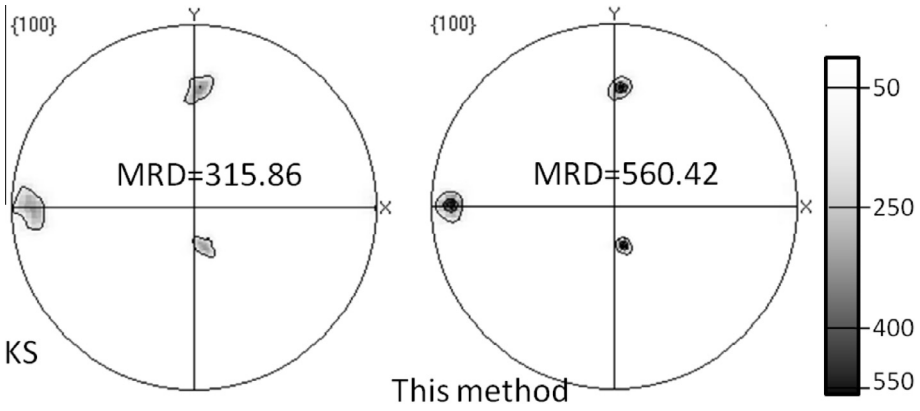

Fig. 4. $\{100\}\gamma$ Pole figure of the austenite grain reconstructed using KS OR and the OR determined by the XABX method.

Table 2. γ Texture intensities expressed in terms of MRD as a function of the OR used to calculate the parent orientation (data from the α EBSD map of Fig. 3a).

Parent γ orientations calculated with OR	KS	NW	GT	This method
MRD	315.86	420.31	498.66	560.42

case with noise. The resulting gradient of the parent γ EBSD map (globally of ~30°) is visualized using the color key of the fundamental zone (also called standard triangle) relative to a specific direction (Fig. 2a). In order to highlight the orientation gradient[1], the direction was chosen so that its projection falls into the center of the fundamental zone. The gradient is also visible on the pole figures (Fig. 2d). The resulting noise and gradient along the black line of Fig. 2a are shown in the misorientation profile in Fig. 2b.

The thin black lines (Fig. 2c) separate domains which transformed into different variants. In this simulation, the orientations of these variants (Fig. 2c and d) were obtained from relation (1) with KS OR ($\Delta g = (5.77°, 48.12°, 5.77°)$). The XABX method was applied to determine the OR at the 12 triple points of Fig. 2c. Finally the ORs have been averaged to obtain a mean result for the grain. The average OR from data without noise is $\Delta g = (5.55°, 48.17°, 5.94°)$ corresponding to eigenvectors having λ_4 always lower than 6×10^{-6}. The calculated OR is only at 0.17° from KS OR. This small difference results from our first hypothesis (Eq. (3)). In such a case, the small orientation variation of the parent at the triple point has little influence on the determination of the OR.

The result in case of noise perturbation is $\Delta g = (5.42°, 48.1°, 6.05°)$ with λ_4 always lower than 2×10^{-4}. This result is at 0.3° from KS OR. The addition of a quasi-white noise has also only a small effect on the OR determination. Moreover, the noise can be smoothed if each misorientation $[g_\alpha(r_j)]^{-1}[g_\alpha(r_i)]$ taken at the triple point is replaced by the misorientation averaged along the boundaries: $\overline{[g_\alpha(r_{jGB})]^{-1}[g_\alpha(r_{iGB})]}$. All the results are summarized in Table 1.

[1] The color key of the fundamental zone is sensitive to the orientation. For example, almost no gradient is perceptible by eye for orientations lying at 15° from the cube orientation (0,0,0).

4.2. Application to ausformed martensite in low carbon steel

In this second example, a steel (wt.% 0.2C, 2Mn) has been ausformed by torsion ($\varepsilon = 0.35$) in the γ domain ($T = 950$ °C). One specimen was water quenched just after deformation; the other was maintained at 950 °C to recrystallize for 15 s before quenching. In order to improve the EBSD data acquisition, both samples were tempered at 300 °C for 300 s. EBSD maps were acquired with a step size of 0.5 μm in a JEOL 6500F FEG SEM equipped with a Nordlys-S EBSD camera from Oxford Instruments. The integration time on the camera was 14 μs. Frames were not averaged. A 8×8 binning and a resolution of the Hough transform of 50 were used.

Within the recrystallized sample, a large grain was identified (Fig. 3a). The grain was equiaxed and contained several twins (which have been excluded from our dataset). The orientations of the martensite variants are expressed in the $\{100\}$ pole figure (Fig. 3b). The three rings are the so-called Bain circles [11]. From this dataset, 1582 triplets of neighbors having distinct misorientations were considered. $\lambda_{4CRIT} = 0.001$ was chosen and only ORs in the KS–NW–Pitch domain have been considered. 188 triplets gave a unique OR, 288 gave multiple solutions and the rest gave either no solutions or solutions out of the considered domain.

It turns out that the value of λ_4 (E in Eq. (8)) is proportional to the square of a deviation to Eq. (7). On the other hand when a unique OR was found, we have calculated the orientations of the three corresponding parents $g_\gamma(r_i)$ and the misorientation angles in between. The average misorientation angle ω is intrinsically function of the deviations between the left and right members of Eqs. (7). In this application example we found the following empirical relation between λ_4 and ω:

$$\lambda_4 = (0.157\omega)^2, \quad \omega \text{ in degrees.} \tag{9}$$

In the considered case, the average of these ORs calculated by our method is $\Delta g = (3.33°, 46.3°, 6.17°)$ which is close to GT OR ($\Delta g = 2.68°, 47.06°, 7.57$). Nevertheless the local determined ORs may deviate from the average within a maximum deviation of 2.2°. This suggests that (i) the OR may vary with the location within the grain [12] or (ii) some plasticity may be induced in the austenite during transformation and our model does not account for it [13]. Each mechanism warps the OR perception and calculation.

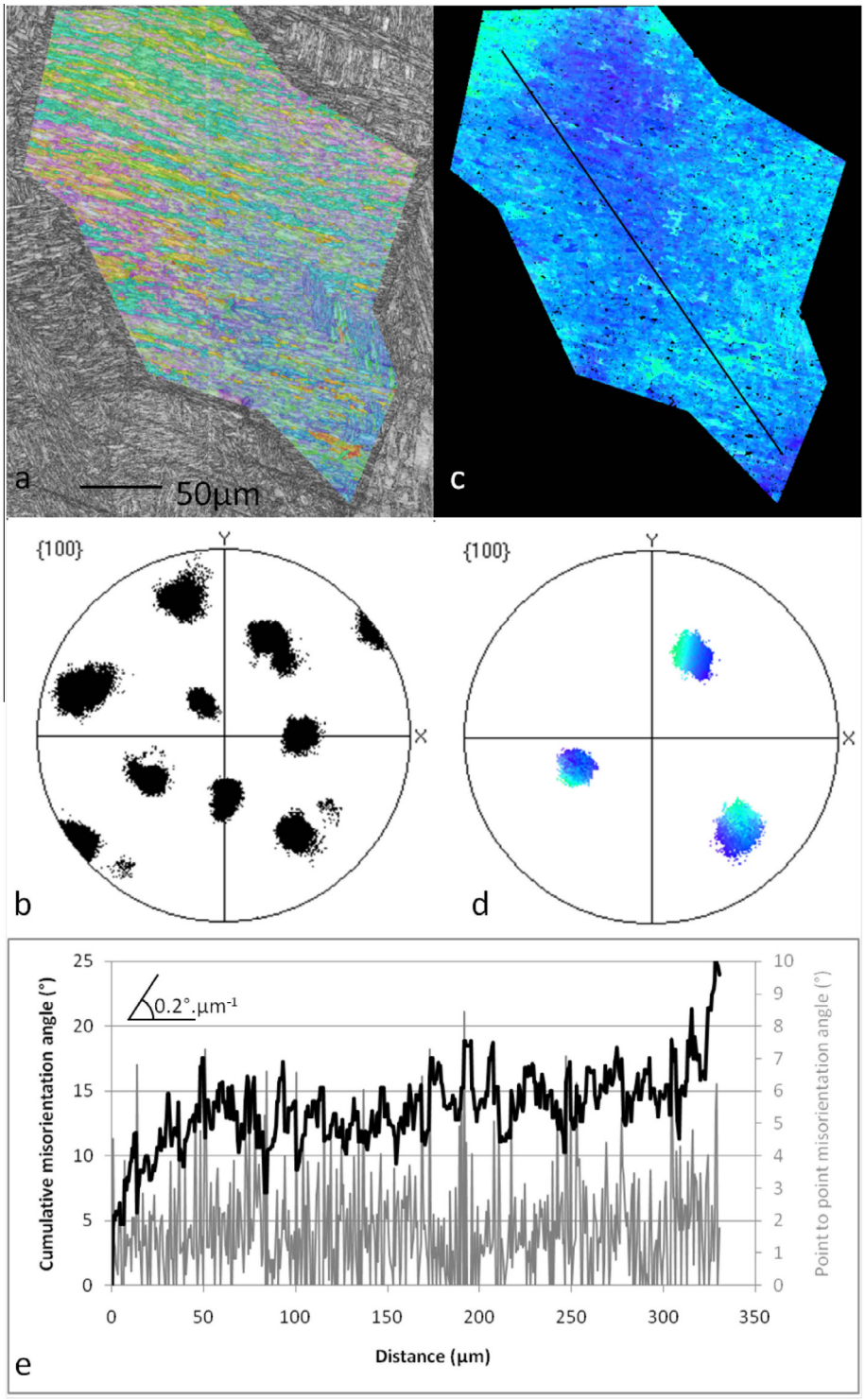

Fig. 5. (a) EBSD map of α variants in a deformed parent γ grain, (b) {100} pole figure of the α variants, (c) the reconstructed γ grain, (d) {100} pole figure of the reconstructed γ grain, (e) misorientation profiles along the black line in (c).

In spite of this, the mean OR can be used to assess the parent orientation. As a matter of fact, knowing the OR and using equations of type (1), it is possible to determine the effective involved symmetry elements $C(r_i)$ by the correlation technique (e.g. [14]). Further, it is possible to calculate for each pixel the parent orientation $[g_\gamma(r_i)]$ from $[g_\alpha(r_i)]$.

Fig. 3c displays the recalculated $[g_\gamma(r_i)]$ orientations of the parent grain. We have also calculated the (100) pole figure of the γ parent grain with the determined OR and for comparison the pole densities from the parent grain recalculated with KS, NW and GT ORs. Two pole figures are given as examples in Fig. 4 and all the results are summarized in Table 2. The pole figure presenting the highest density (i.e. the least spread) is the most consistent with the actual state of parent grain (recrystallized grain) for which the orientation variation should remain very weak. Indeed, Fig. 4 and Table 2 show that the calculation performed with the OR determined by the XABX method

Table 3. γ Texture intensities expressed in terms of MRD as a function of the OR used to calculate the parent orientation (data from the α EBSD map of Fig. 5a).

Parent γ orientations calculated with OR	KS	NW	GT	This method
MRD	193.69	251.70	315.38	321.52

gives the highest density (560 in terms of multiple of random distribution (MRD)).

In a recrystallized γ grain, one would expect to have a single orientation in the whole grain. One can see that the spread of the orientations within the grain is quite large (Fig. 3d). The cumulative misorientation profile (Fig. 3e) along the black straight line of Fig. 3c is flat in mean, showing that in average the orientation is constant within the grain. However, a variation of $\sim\pm4°$ appears because of the same two reasons explained earlier: (i) the local OR may vary [12] and/or (ii) some plasticity may be induced in the austenite during transformation and our model does not account for it [13]. Nevertheless the OR determined by the XABX method is the best estimate of the mean OR within the grain among the other tested ORs.

The same type of analysis was applied to a deformed austenite grain. The grain isolated in the EBSD map of the deformed material is shown in Fig. 5a. The orientations are expressed in the corresponding (100) pole figure (Fig. 5b). Two differences with the previous example appear: (i) the Bain circle are not easily distinguishable; (ii) a large orientation gradient is present. 2038 triplets of neighbors had distinct misorientations. A unique OR was found for 128 triplets. The average of theses ORs is equal to $\Delta g = (3.23°, 47°, 7.4°)$, which is very close to the mean OR obtained in the previous example and also to GT OR. The reconstruction of the EBSD map of the γ grain, using the method previously cited with the mean OR calculated, is presented in Fig. 5c. The color variation reports the orientation gradient. As in the previous example, the {100} pole figures of the parent γ grain recalculated according to KS, NW and GT ORs have been also calculated. The results are presented in Table 3. The highest densities are obtained with the XABX OR determination (MRD = 321) and GT OR (MRD = 315). The highest densities are lower than in the previous case and the dispersion is larger. These features are consistent with the deformed state of the sample. The misorientation profile (Fig. 5e) along the black straight line of Fig. 5c logically translates the presence of an orientation gradient even though it may only mark a trend. The cumulative misorientation angle of 26° gives an idea of the magnitude of the orientation gradient in the grain. The steepest slope is $0.2° \ \mu m^{-1}$ and the orientation gradient across two pixels remains low. The hypothesis (Eq. (3)) of constancy of the parent orientation in the immediate vicinity is therefore a good approximation.

5. Conclusion

We demonstrate that it is possible to evaluate the OR from the child orientations even if the parent orientation is unknown and not constant. Three misorientations determined at locations close to the boundaries of three variants or at a triple junction, allow the establishment of an equation system in which the OR is the main unknown to be solved if the following two assumptions are met: (1) the parent orientation gradient is weak in a narrow vicinity; (2) the local ORs remain close to a mean OR.

It is shown here that the first hypothesis even in a globally strong orientation gradient (in a deformed grain) is not limiting.

Our investigations on real materials show that even if the second hypothesis is not fulfilled everywhere in the grain, a relevant mean OR may be obtained by averaging the ORs determined for all analyzed triplets.

This approach opens the way for research on local variability of OR as a function of processing conditions and allows effective OR to be used in the reconstruction of parent microstructures from the child ones.

Appendix A

Finding the OR from variants requires developing tools to solve matrix equations of the type:

$$X \cdot A_i = B_i \cdot X. \tag{A.1}$$

where A_i and B_i are known rotation matrices, whereas X is the rotation matrix to be found.

The resolving method used owes much to the reading of Ref. [15].

The quaternion formulation of Eq. (A.1) allows the solving to be very efficient, as shown in the following. Eq. (A.1) is equivalent to the quaternion equation

$$Q_X * Q_{A_i} = Q_{B_i} * Q_X \tag{A.2}$$

with $Q = [q_0, q_1, q_2, q_3]^T$ (q_0 being the real part of the quaternion and q_1, q_2, q_3 the imaginary part) and where Q_X stands for X, Q_{A_i} for A_i and Q_{B_i} for B_i.

On the other hand, the quaternion multiplication can be written in matrix form such as:

$$Q_X * Q_{A_i} = \overline{M}(Q_{A_i})Q_X$$

$$Q_{B_i} * Q_X = M(Q_{B_i})Q_X$$

with matrices $M(Q)$ and $\overline{M}(Q)$ equal to:

$$M(Q) = \begin{bmatrix} q_0 & -q_1 & -q_2 & -q_3 \\ q_1 & q_0 & -q_3 & q_2 \\ q_2 & q_3 & q_0 & -q_1 \\ q_3 & -q_2 & q_1 & q_0 \end{bmatrix} \quad \text{and}$$

$$\overline{M}(Q) = \begin{bmatrix} q_0 & -q_1 & -q_2 & -q_3 \\ q_1 & q_0 & q_3 & -q_2 \\ q_2 & -q_3 & q_0 & q_1 \\ q_3 & q_2 & -q_1 & q_0 \end{bmatrix}$$

With this modification, Eq. (A.2) can be substituted by:

$$\left(\overline{M}(Q_{A_i}) - M(Q_{B_i})\right)Q_X = 0 \tag{A.3}$$

The square norm of the corresponding error is given by:

$$\begin{aligned} \|\left(\overline{M}(Q_{A_i}) - M(Q_{B_i})\right)Q_X\|^2 &= Q_x^T \left(\overline{M(Q_{Ai})} - M(Q_{Bi})\right)^T \left(\overline{M(Q_{Ai})} - M(Q_{Bi})\right)Q_X \\ &= Q_X^T S_i Q_X \end{aligned} \tag{A.4}$$

As discussed in Section 3, the unique solution X can be only found from a set of equations $X \times A_i = B_i \times X$.

Therefore the error function that allows Q_X to be computed reads:

$$E(Q_X) = \sum_i Q_X^T S_i Q_X = Q_X^T \left(\sum_i S_i \right) Q_X = Q_X^T S Q_X \qquad \text{(A.5)}$$

Finding the Q_X solution of Eq. (A.2) amounts to minimizing $E(Q_X)$ with the constrain $\|Q_X\| = 1$.

For this, a Lagrange multiplier λ can be used:

$$Min\left(Q_X^T S Q_X + \lambda(1 - Q_X^T Q_X)\right) \qquad \text{(A.6)}$$

This function reaches a minimum when its first derivative is null. This leads to:

$$S Q_X = \lambda Q_X$$

It is easy to see that

$$Min(E(Q_X)) = Min\left(Q_X^T S Q_X\right) = \lambda \qquad \text{(A.7)}$$

The four eigenvalues λ of S and their corresponding eigenvectors are calculated. The eigenvalue closest to zero is retained because it minimizes the error function (A.5) and its corresponding eigenvector Q_X determines the solution X.

References

[1] B. Gardiola, C. Esling, M. Humbert, K.-E. Hensger, Adv. Eng. Mater. 5 (2003) 583.
[2] A. Lambert-Perlade, A.F. Gourgues, A. Pineau, Acta Mater. 52 (2004) 2337.
[3] G. Nolze, Cryst. Res. Technol. 41 (2006) 72.
[4] G. Nolze, Cryst. Res. Technol. 43 (2008) 61.
[5] Y. He, S. Godet, P.J. Jacques, J.J. Jonas, Acta Mater. 54 (2006) 1323.
[6] C. Cabus, H. Réglé, B. Bacroix, Mater. Charact. 58 (2007) 332.
[7] Bhadeshia et al., Int. J. Mater. Res. 99 (2008) 342.
[8] G. Miyamoto, N. Takayama, T. Furuhara, Scr. Mater. 60 (2009) 1113.
[9] M. Humbert, P. Blaineau, L. Germain, N. Gey, Scr. Mater. 64 (2011) 114.
[10] B.K.P. Horn, J. Opt. Soc. Am. A 4 (1987) 629.
[11] Y. He, S. Godet, J. Jonas, J. Appl. Cryst. 39 (2006) 72.
[12] H. Sato, S. Zaefferer, Acta Mater. 57 (2009) 1931.
[13] A.F. Gourgues-Lorenzon, Int. Mater. Rev. 52 (2007) 65.
[14] L. Germain, N. Gey, R. Mercier, P. Blaineau, M. Humbert, Acta Mater. 60 (2012) 4551.
[15] F. Dornaika, R. Horaud, IEEE Trans. Rob. Autom. 14 (4) (1998) 617–622.